

Gravitational Wave Polarization Detection with Pyramid Constellation of Gravitational Wave Observatory

Hong-Bo Jin^{1,2} and Cong-Feng Qiao^{2,3}

¹National Astronomical Observatories, Chinese Academy of Sciences, Beijing 100101, China

²The International Centre for Theoretical Physics Asia-Pacific, University of Chinese Academy of Sciences, Beijing 100190, China

³The School of Physical Sciences, University of Chinese Academy of Sciences, Beijing 100049, China

For the first time, we have introduced the Pyramid Constellation of Gravitational Wave Observatory (PCGO) for GW polarization detection. The PCGO is composed of four identical spacecrafts (S/Cs). The laser telescopes and their pointing structures are mounted on the S/C platform and are evenly distributed at three locations 120 degrees apart. Compared to a three-S/C configuration, the addition of a fourth S/C and its mounted telescope serve as redundant backups, especially for the telescopes, which together with the other two telescopes, automatically form a stable mass center for the platform without the need for trim mass. Since the radial distance of S/C4 is greater than that of the other spacecraft, the three arm lengths associated with S/C4 change significantly over a one-year period. Time delay interferometry (TDI) has been proven effective for suppressing frequency noise in this context. The unequal arm Michelson TDI configuration and the Sagnac TDI configuration are equally effective for eliminating the laser frequency noise based on the PCGO configuration. Compared to the configurations of LISA, Taiji, and TianQin, the PCGO has more combinations of optical paths in its TDI system, offering greater sensitivity to GW signals. The configuration of PCGO is simultaneously sensitive to the six polarization modes of GWs, which means that it allows for greater flexibility in extracting the polarization components from the total GW polarization signals.

In general relativity (GR), GW polarization modes are tensor named as plus and cross modes, which have been detected from the LIGO, Virgo, and KAGRA collaborations^{1,2}. The other GW modes beyond GR, called as two scalar polarization modes and two vector modes, have being probed especially with an expected network of Advanced LIGO, Advanced Virgo, and KAGRA^{3,4}. The ability of Taiji to detect the polarization modes is explored in the parametrized post-Einsteinian framework and it is found that Taiji can measure the dipole and quadruple emission of GWs⁵. The performance of the LISA-TianQin network for detecting polarizations of stochastic GW background is also investigated⁶.

In the six polarizations of GWs in a general metric theory of gravitation in four dimensions, the additional polarizations mean that the theory of gravitation should be extended beyond GR, and excludes some theoretical models, depending on which polarization modes are detected⁷. Thus, the observation of the GW polarizations is used to probe the extended law of gravity and extra

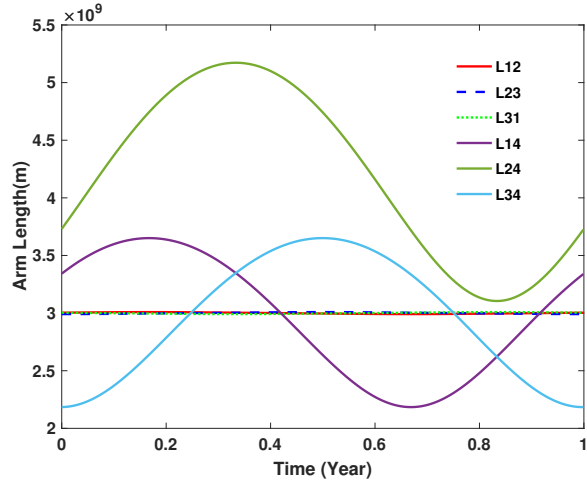
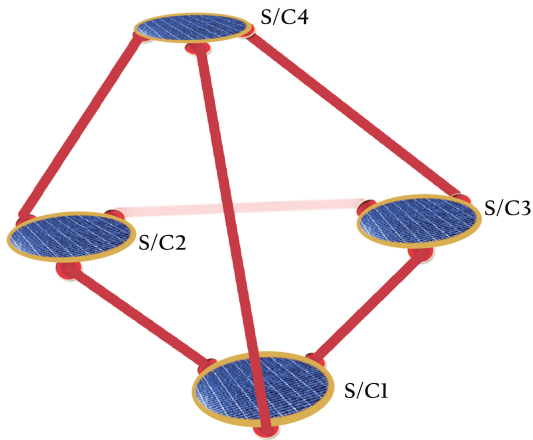


Figure 1: (left) The schematic of the pyramid constellation of gravitational wave observatory(PCGO). There are four identical S/Cs. The orientation of the laser beam is adjusted by the telescope pointing structure, which is integrated with the telescope and evenly distributed at three locations 120 degrees apart in the spacecraft platform. (right) Variations of the arm lengths (Laser path distance between S/Cs) in 1 year. In the legend, L_{mn} is between the S/C_m and S/C_n. When mn is 12, it is L12.

dimensions. The six polarizations of GWs response to the detector of GWs in four-dimensional space, which favors the tridimensional detector of GWs. That is attained from the recent studies of the network of some observatories, such as LIGO, Virgo, and KAGRA or LISA, Taiji and TianQin, etc.

In this paper, we propose the pyramid constellation of gravitational wave observatory(PCGO) with a four triangles composed of four S/Cs for the three-dimensional configuration different from those networks. The orientation of the laser beam is adjusted by the telescope pointing structure, which is integrated with the telescope and evenly distributed at three locations 120 degrees apart in the spacecraft platform. Compared to the three S/Cs configuration, the addition of S/C and the mounted telescope are also seen as redundant backups, especially for a telescope, which automatically form a stable mass center of platform with the other two telescopes without the trim mass. This configuration of PCGO is shown in the left of Figure 1. The arm lengths of triangles composed of three S/Cs: S/C1 - S/C3 have almost same values. The other arm lengths of triangles composed of three S/Cs with S/C4 and S/C1 - S/C3 have the variable values in one year period. That is derived from the S/C4 has a longer radial distance than the other S/Cs. The orbit details of S/Cs are found in the Method section. In the right of Figure 1, the arm lengths between SCs are drawn in one year period.

In the space-based observatories with a triangle of three spacecrafts, such as LISA⁸, Taiji⁹ and TianQin^{10,11}, the laser frequency noise are dominant. The heterodyne interferometry with

unequal arm lengths and independent phase-difference readouts has been proposed to cancel the frequency noise^{12,13}. The properly time-shifting and linearly combining independent Doppler measurements are applied, which has been called time-delay interferometry (TDI)^{12,13}. In the paper¹⁴, the optical path differences of the second-generation TDI were calculated for LISA, TAIJI, and LISA-like missions, which are well below their respective limits which the laser frequency noise is required to be suppressed. Compared to those triangular detectors, PCGO has more than four times combinations of optical paths of time delay interferometer(TDI) to suppress the frequency noise. In this paper, based on the unequal arm Michelson TDI configuration and the Sagnac TDI configuration for three S/Cs, the optical path differences of the second-generation TDI are calculated to check the capability of TDI for the apparently variable arm lengths. As is seen in Figure 2, Michelson TDI configuration is from the optical path combination of two arms and the optical path differences are below the limits of noise canceling, compared to the results in the paper¹⁴. In the optical path differences of all the combination, the values relevant to the combination between S/C1, S/C2 and S/C3 are 1% less than the others, which is seen in the Figure 2. This result is due to the fact that, in one year period, three arm lengths relevant to S/C4 are changed apparently, that is seen in the right of Figure 1.

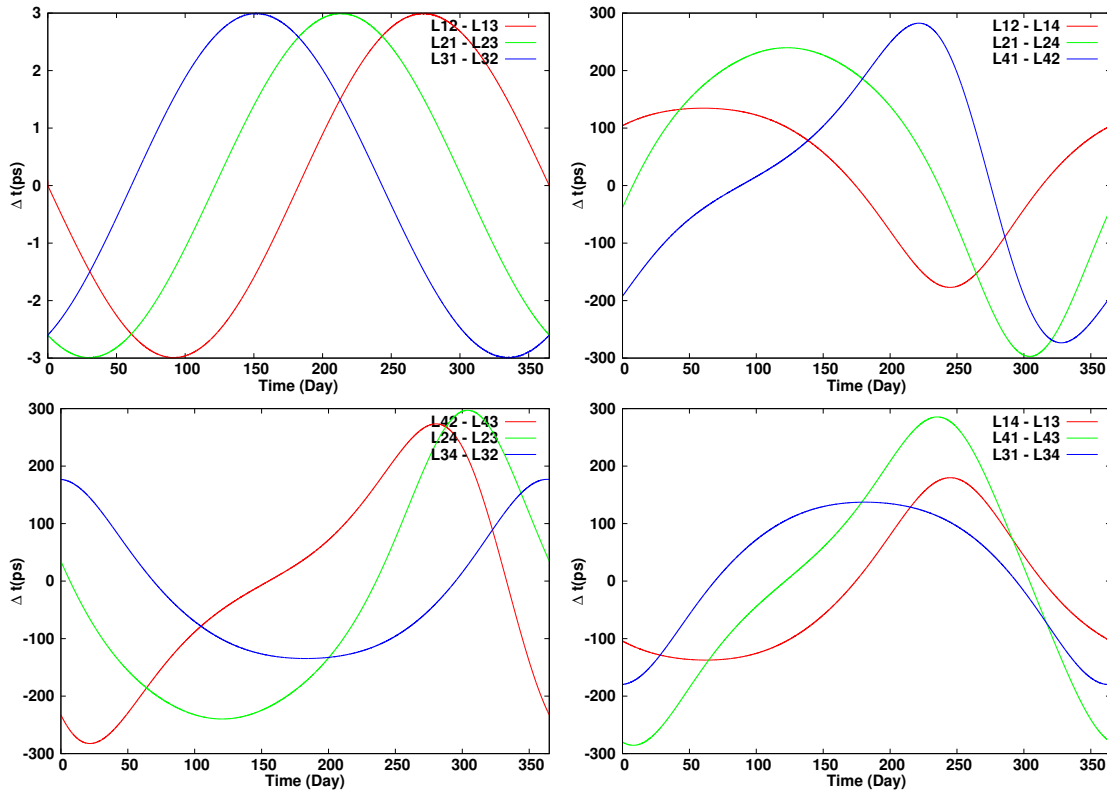


Figure 2: The optical path differences of the second-generation Michelson TDI in one year period. The unit of the y-coordinate is the picosecond (ps) and the optical path difference is $C\Delta t$. C is light speed. As an example, in the legend, L12 - L13 means the optical path differences between $S/C1 \rightarrow S/C2 \rightarrow S/C1 \rightarrow S/C3 \rightarrow S/C1$ and $S/C1 \rightarrow S/C3 \rightarrow S/C1 \rightarrow S/C2 \rightarrow S/C1$.

In the Sagnac TDI configuration for three S/Cs, the optical path differences of the second-generation TDI are shown in Figure 3 and 4. In one triangle of S/C1, S/C2, and S/C3, the optical path differences are roughly 1/10 less than Michelson TDI and the other optical path differences are consistent with the ones relevant to Michelson TDI, which is shown in Figure 3. That is derived from the variable arm lengths relevant to S/C4. When the combinations of Sagnac TDI are in two triangles of S/Cs, the optical path differences of the double combinations are almost close to the one triangles of S/Cs. The results and combinations are found in Figure 4.

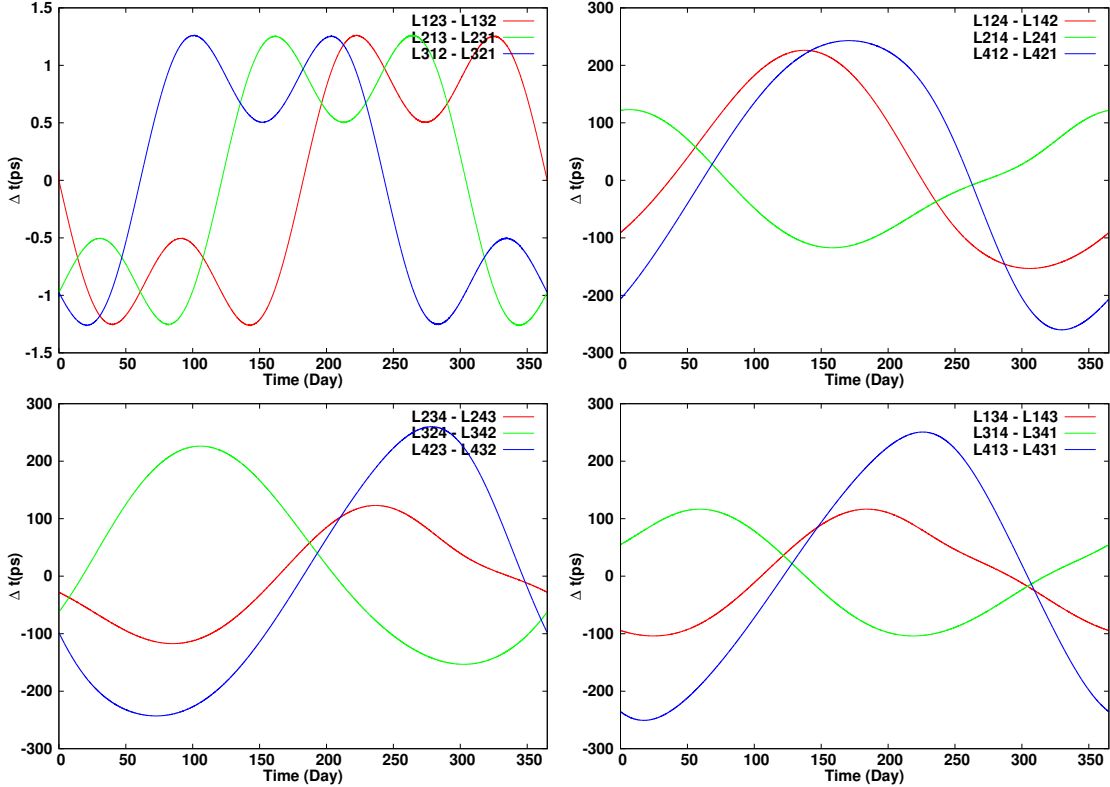


Figure 3: The optical path differences of the second-generation Sagnac TDI in one triangle of S/Cs in one year period. The unit of the y-coordinate is the picosecond (ps) and the optical path differences is $C\Delta t$. C is light speed. As an example, in the legend, L123 - L132 means the optical path differences between $S/C1 \rightarrow S/C2 \rightarrow S/C3 \rightarrow S/C1 \rightarrow S/C3 \rightarrow S/C2 \rightarrow S/C1$ and $S/C1 \rightarrow S/C3 \rightarrow S/C2 \rightarrow S/C1 \rightarrow S/C2 \rightarrow S/C3 \rightarrow S/C1$.

In summary, as the radial distance of S/C4 is longer than the other S/Cs, three arm lengths relevant to S/C4 are changed apparently in one year period. The second-generation TDI are selected to eliminate the laser frequency noise, instead of the first generation TDI. Compared to the optical path differences shown in Figure 2, 3 and 4, the unequal arm Michelson TDI configuration and the Sagnac TDI configuration for three S/Cs are equally effective for elimination of the laser frequency noise.

As the periodic motion of GW detectors on the solar orbit exists, the amplitude of GW source

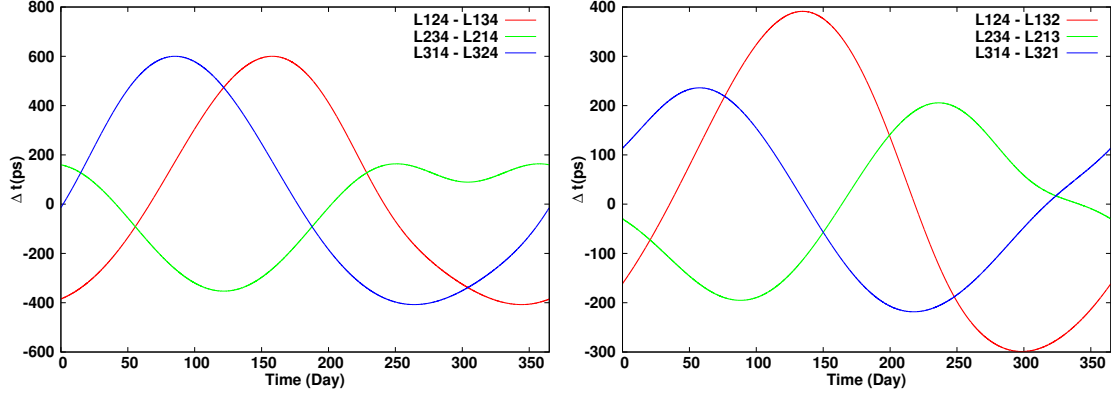


Figure 4: The optical path differences of the second-generation Sagnac TDI in two triangles of S/Cs in one year period. The unit of the y-coordinate is the picosecond (ps) and the optical path differences is $C\Delta t$. C is light speed. As an example, in the legend, L124 - L134 means the optical path differences between $S/C1 \rightarrow S/C2 \rightarrow S/C4 \rightarrow S/C1 \rightarrow S/C3 \rightarrow S/C4 \rightarrow S/C1 \rightarrow S/C4 \rightarrow S/C2 \rightarrow S/C1 \rightarrow S/C4 \rightarrow S/C3 \rightarrow S/C1$ and $S/C1 \rightarrow S/C4 \rightarrow S/C2 \rightarrow S/C1 \rightarrow S/C4 \rightarrow S/C3 \rightarrow S/C1 \rightarrow S/C2 \rightarrow S/C4 \rightarrow S/C1 \rightarrow S/C3 \rightarrow S/C4 \rightarrow S/C1$.

at a sky position is modulated with the detector position on orbit in one year period. Obviously, the polarization directions of GWs relative to detector are also changed with the detector position on orbit. Furthermore, when a detector arrives at a position on orbit, some polarizations of GW sources may be not detected where a polarization direction of GWs is perpendicular to an arm of GW detector.

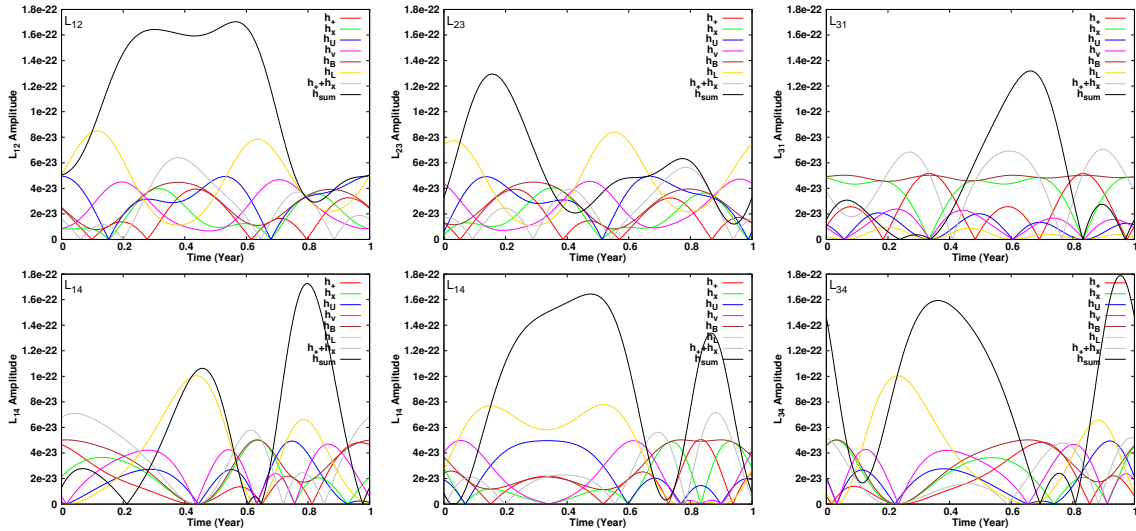


Figure 5: Amplitude of six polarization modes of GW source: J0806 response to all the detector arms in one year period. As an example, L_{12} means the arm between S/C1 and S/C2.

A verification white dwarf binary signal: J0806 as the identified source is selected, whose

parameters are detailed in the paper¹⁵. The polarization angle is set $\psi = 0$, and initial orbital phase is set $\phi_0 = 0$. The sky location parameters $\phi[rad]$, $\beta[rad]$ and $D_L[kpc]$ are 2.1021, -0.0821 and 5 respectively¹⁵. As a monochromatic source, The GW waveform of J0806 is calculated using the quadrupole approximation^{16,17}. Based on this approximation, the gravitational wave signals are described as a combination of the two polarizations ($+$, \times)¹⁸ and the other four components of GW polarizations cannot be calculated with that approximation. In this paper, the GW waveforms relevant to the other four components of GW polarizations are set to be equal to the (\times) component, artificially. That is an independent model. The details are found in the subsection of Method section: GW Signal Model. The every components of GW polarization expression in the subsection of Method section: Polarization Modes.

As is seen in Figure 5, all the detector arms are simultaneously sensitive to the six polarization modes of GWs. The arms between SC4 and S/C1-S/C3 have GW responses different from the arms between S/C1, SC2 and S/C3. The h_{sum} means the amplitude of GW response to detector arm, which is an observable quantity. In the response intensity of six detector arms, h_{sum} changes with the detector position on orbit in one year period. The newly added three arms have a different response of GWs from the triangle arms, compared to LISA, Taiji and Tianqin. That indicates that there are more freedoms for the polarization component extraction from the total signals of GWs.

In conclusion, the Pyramid Constellation of Gravitational Wave Observatory (PCGO) is a novel system comprising four spacecrafts (S/Cs) that enhances sensitivity to gravitational wave polarizations beyond traditional ground-based or space observatories like LIGO, Virgo, KAGRA, LISA, Taiji, and TianQin. The laser telescopes and their pointing structures are mounted on the S/C platform and are evenly distributed at three locations 120 degrees apart. Compared to a three-S/C configuration, the addition of a fourth S/C and its mounted telescope serve as redundant backups, especially for the telescopes, which together with the other two telescopes, automatically form a stable mass center for the platform without the need for trim mass. The PCGO employs more combinations of time delay interferometry configurations to effectively suppress laser frequency noise, offering more sensitivity to gravitational wave signals. As the configuration of PCGO is simultaneously sensitive to the six polarization modes of GWs, the PCGO allows for greater flexibility in extracting polarization components from total GW signals, making it simultaneously sensitive to all six polarization modes of gravitational waves.

Methods

Detector Orbit Referring to LISA orbit, S/Cs of PCGO orbit Kepler¹⁹ and the arm length is $L=3 \times 10^9$ m between S/C1, S/C2 and S/C3. Each spacecraft (S/C) positions are expressed as a function of time. To second order in the eccentricity, the Cartesian coordinates of the spacecraft are given by

$$\begin{aligned}
 x(t) &= R \cos(\alpha) + \frac{1}{2}eR \left(\cos(2\alpha - \beta) - 3 \cos(\beta) \right) \\
 &\quad + \frac{1}{8}e^2R \left(3 \cos(3\alpha - 2\beta) - 10 \cos(\alpha) - 5 \cos(\alpha - 2\beta) \right) \\
 y(t) &= R \sin(\alpha) + \frac{1}{2}eR \left(\sin(2\alpha - \beta) - 3 \sin(\beta) \right) \\
 &\quad + \frac{1}{8}e^2R \left(3 \sin(3\alpha - 2\beta) - 10 \sin(\alpha) + 5 \sin(\alpha - 2\beta) \right) \\
 z(t) &= -\sqrt{3}eR \cos(\alpha - \beta) + \sqrt{3}e^2R \left(\cos^2(\alpha - \beta) + 2 \sin^2(\alpha - \beta) \right) \quad (1)
 \end{aligned}$$

Where $R = 1$ AU is the radial distance to the center of the triangle from S/C1 to S/C3. For S/C4 above the triangle R is $(1 + 0.0163738)$ AU. 0.0163738 is best-fit value when the mean value of arm length is near $L=3 \times 10^9$ m in 1 year. $\alpha = 2\pi t/\text{year} + \kappa$ is the orbital phase of the guiding center, and $\beta = 2\pi m/3 + \lambda$ ($m = 0.0, 1.0, 2.0, 2.5$) is the relative phase from S/C1 to S/C4. The parameters κ and $\lambda = 0$ give the initial ecliptic longitude and orientation of constellation. The orbital eccentricity e is computed based on the arm length: $e = L/(2\sqrt{3}R)$. By setting the mean arm-length equal to those of the TAJI baseline, $L = 3 \times 10^9$ m, the spacecraft orbits are found to have an eccentricity of $e = 0.005789$, which indicates that the second order effects are down by a factor of 100 relative to leading order.

GW Signal Model of white dwarf J0806 The gravitational wave signals from white dwarf binary are described by a set of eight parameters: frequency f , frequency derivative \dot{f} , amplitude \mathcal{A} , sky position in ecliptic coordinates (λ, β) , orbital inclination ι , polarisation angle ψ , and initial orbital phase ϕ_0 ^{20–22}. The recipes for generating \mathcal{A} , f , \dot{f} , and (λ, β) are based on the currently available observations. The gravitational wave emitted by a monochromatic source is calculated using the quadrupole approximation^{16,17}. In this approximation, the gravitational wave signals are described as a combination of the two polarizations $(+, \times)$ ¹⁸:

$$\begin{aligned}
 h_+(t) &= \mathcal{A}(1 + \cos^2 \iota) \cos(\Phi(t)) \\
 h_\times(t) &= 2\mathcal{A} \cos \iota \sin(\Phi(t)). \quad (2)
 \end{aligned}$$

In above expression,

$$\begin{aligned}
 \mathcal{A} &= \frac{2(GM)^{5/3}}{c^4 D_L} (\pi f)^{2/3} \\
 \Phi(t) &= 2\pi f t + \pi \dot{f} t^2 + \phi_0 \\
 \dot{f} &= \frac{96}{5} \pi^{8/3} \left(\frac{GM}{c^3} \right)^{5/3} f^{11/3}. \quad (3)
 \end{aligned}$$

where $\mathcal{M} \equiv (m_1 m_2)^{3/5} / (m_1 + m_2)^{1/5}$ is the chirp mass, and D_L is luminosity distance, and G and c are the gravitational constant and the speed of light, respectively.

A verification white dwarf binaries signals: J0806 as the identified sources are selected, whose parameters are detailed in the paper¹⁵. The polarization angle is set $\psi = 0$, and initial orbital phase is set $\phi_0 = 0$. The sky location parameters $\phi[rad]$, $\beta[rad]$ and $D_L[kpc]$ are 2.1021, -0.0821 and 5 respectively¹⁵. Except for two polarizations (+, \times), the other four components of GW polarizations cannot calculated with quadrupole approximation^{16,17}. In this paper, the GW waveforms relevant to the other four components of GW polarizations are set to be equal to (\times) component, artificially.

Polarization Modes In four dimension space-time, GWs have six polarization modes: two transverse-traceless modes [plus (+) and cross (\times)], two vector longitudinal modes (U and V), a scalar transverse breathing mode (B), and a scalar longitudinal mode (L). The total tensor with all six polarization modes is written as

$$\mathbf{H}(t) = h_+(t)\epsilon^+ + h_\times(t)\epsilon^\times + h_U(t)\epsilon^U + h_V(t)\epsilon^V + h_B(t)\epsilon^B + h_L(t)\epsilon^L, \quad (4)$$

where ϵ^A ($A = +, \times, U, V, B, L$) are the polarization tensors and h_A are the waveforms of the polarization modes.

Solar System Barycenter (SSB) frame, based on the ecliptic plane, is selected. In SSB frame, the standard spherical coordinates (θ, ϕ) and the associated spherical orthonormal basis vectors ($\mathbf{e}_r, \mathbf{e}_\theta, \mathbf{e}_\phi$) are confirmed. The position of the source in the sky is parametrized by the ecliptic latitude $\beta = \pi/2 - \theta$ and the ecliptic longitude $\lambda = \phi$. The gravitational wave propagation vector \hat{k} in spherical coordinates is expressed as

$$\hat{k} = -\mathbf{e}_r = -\cos \beta \cos \lambda \hat{\mathbf{x}} - \cos \beta \sin \lambda \hat{\mathbf{y}} - \sin \beta \hat{\mathbf{z}}. \quad (5)$$

The reference polarization vectors is the following:

$$\begin{aligned} \hat{u} &= -\mathbf{e}_\theta = -\sin \beta \cos \lambda \hat{\mathbf{x}} - \sin \beta \sin \lambda \hat{\mathbf{y}} + \cos \beta \hat{\mathbf{z}} \\ \hat{v} &= -\mathbf{e}_\phi = \sin \lambda \hat{\mathbf{x}} - \cos \lambda \hat{\mathbf{y}}. \end{aligned} \quad (6)$$

The polarization tensors are given

$$\begin{aligned} \epsilon^+ &= \mathbf{e}^+ \cos 2\psi - \mathbf{e}^\times \sin 2\psi, \\ \epsilon^\times &= \mathbf{e}^+ \sin 2\psi + \mathbf{e}^\times \cos 2\psi, \\ \epsilon^U &= \mathbf{e}^U \cos \psi - \mathbf{e}^V \sin \psi, \\ \epsilon^V &= \mathbf{e}^U \sin \psi + \mathbf{e}^V \cos \psi, \\ \epsilon^B &= \mathbf{e}^B, \\ \epsilon^L &= \mathbf{e}^L, \end{aligned} \quad (7)$$

where ψ is the polarization angle and the six basis tensors are ⁷

$$\begin{aligned}
\mathbf{e}^+ &= \hat{u} \otimes \hat{u} - \hat{v} \otimes \hat{v}, \\
\mathbf{e}^\times &= \hat{u} \otimes \hat{v} + \hat{v} \otimes \hat{u}, \\
\mathbf{e}^U &= \hat{u} \otimes \hat{k} + \hat{k} \otimes \hat{u}, \\
\mathbf{e}^V &= \hat{v} \otimes \hat{k} + \hat{k} \otimes \hat{v}, \\
\mathbf{e}^B &= \hat{u} \otimes \hat{u} + \hat{v} \otimes \hat{v}, \\
\mathbf{e}^L &= \hat{k} \otimes \hat{k}.
\end{aligned} \tag{8}$$

Acknowledgements We thank Yue-Liang Wu for the theory of GW polarization beyond GR and requirement of the space mission of GW detection. which are value useful to improve the manuscript. This work has been supported by the Fundamental Research Funds for the Central Universities. This work has been supported in part by the Strategic Priority Research Program of the Chinese Academy of Sciences under Grant No. XDA15020701 and XDA15020708. In this paper, The numerical computation of this work was completed at TAIJI Cluster of University of Chinese Academy of Sciences.

1. Abbott, R. *et al.* Gwtc-3: compact binary coalescences observed by ligo and virgo during the second part of the third observing run. *Physical Review X* **13**, 041039 (2023).
2. Abbott, R. *et al.* Open Data from the Third Observing Run of LIGO, Virgo, KAGRA, and GEO. *The Astrophysical Journal Supplement Series* **267**, 29 (2023). URL <https://iopscience.iop.org/article/10.3847/1538-4365/acdc9f.2302.03676>.
3. Hagihara, Y., Era, N., Iikawa, D. & Asada, H. Probing gravitational wave polarizations with Advanced LIGO, Advanced Virgo, and KAGRA. *Physical Review D* **98**, 064035 (2018). URL <https://link.aps.org/doi/10.1103/PhysRevD.98.064035.1807.07234>.
4. Hagihara, Y., Era, N., Iikawa, D., Nishizawa, A. & Asada, H. Constraining extra gravitational wave polarizations with Advanced LIGO, Advanced Virgo, and KAGRA and upper bounds from GW170817. *Physical Review D* **100**, 064010 (2019). URL <https://link.aps.org/doi/10.1103/PhysRevD.100.064010.1904.02300>.
5. Liu, C., Ruan, W.-H. & Guo, Z.-K. Constraining gravitational-wave polarizations with Taiji. *Physical Review D* **102**, 124050 (2020). URL <http://arxiv.org/abs/2006.04413><http://dx.doi.org/10.1103/PhysRevD.102.124050>.
6. Hu, Y., Wang, P.-P., Tan, Y.-J. & Shao, C.-G. Testing the Polarization of Gravitational-wave Background with the LISA-TianQin Network. *The Astrophysical Journal* **961**, 116 (2024). URL <https://iopscience.iop.org/article/10.3847/1538-4357/ad0cef>.
7. Nishizawa, A., Taruya, A., Hayama, K., Kawamura, S. & Sakagami, M.-a. Probing nontensorial polarizations of stochastic gravitational-wave backgrounds with ground-based laser interferometers. *Physical Review D* **79**, 082002 (2009). URL <https://link.aps.org/doi/10.1103/PhysRevD.79.082002.0903.0528>.
8. Amaro-Seoane, P. *et al.* Laser interferometer space antenna. *arXiv preprint arXiv:1702.00786* (2017).
9. Hu, W.-R. & Wu, Y.-L. The taiji program in space for gravitational wave physics and the nature of gravity (2017).
10. Luo, J. *et al.* TianQin: a space-borne gravitational wave detector. *Classical and Quantum Gravity* **33**, 035010 (2015). URL <https://iopscience.iop.org/article/10.1088/0264-9381/33/3/035010><http://arxiv.org/abs/1512.02076>.
11. Mei, J. *et al.* The TianQin project: current progress on science and technology. *Progress of Theoretical and Experimental Physics* **2021**, 05A107 (2020). URL <https://academic.oup.com/ptep/article/doi/10.1093/ptep/ptaa114/5880559><https://arxiv.org/abs/2008.10332>.

12. Dhurandhar, S., Ni, W.-T. & Wang, G. Numerical simulation of time delay interferometry for a LISA-like mission with the simplification of having only one interferometer. *Advances in Space Research* **51**, 198–206 (2013). URL <https://linkinghub.elsevier.com/retrieve/pii/S0273117712005893>. 1102.4965.
13. Tinto, M. & Dhurandhar, S. V. Time-Delay Interferometry. *Living Reviews in Relativity* **17**, 6 (2014). URL <https://link.springer.com/10.12942/lrr-2014-6>.
14. Wang, G. & Ni, W.-T. Numerical simulation of time delay interferometry for TAIJI and new LISA. *Research in Astronomy and Astrophysics* **19**, 058 (2019). URL <http://arxiv.org/abs/1707.09127><http://dx.doi.org/10.1088/1674-4527/19/4/1707.09127>.
15. Kupfer, T. *et al.* LISA verification binaries with updated distances from Gaia Data Release 2. *Monthly Notices of the Royal Astronomical Society* **480**, 302–309 (2018). URL <https://academic.oup.com/mnras/article/480/1/302/5037945>. 1805.00482.
16. Landau, L. D. & Lifshitz, E. M. *The classical theory of fields; 2nd ed.* Course of theoretical physics (Pergamon, London, 1962). URL <https://cds.cern.ch/record/101809>.
17. Peters, P. C. & Mathews, J. Gravitational Radiation from Point Masses in a Keplerian Orbit. *Phys. Rev.* **131**, 435–440 (1963). URL <https://link.aps.org/doi/10.1103/PhysRev.131.435>.
18. Korol, V., Hallakoun, N., Toonen, S. & Karnesis, N. Observationally driven Galactic double white dwarf population for LISA. *Monthly Notices of the Royal Astronomical Society* **511**, 5936–5947 (2022). URL <http://arxiv.org/abs/2109.10972><http://dx.doi.org/10.1093/mnras/stac415><https://academic.oup.com/mnras/advance-article-abstract/doi/10.1093/mnras/stac415/6644441>. 2109.10972.
19. Rubbo, L. J., Cornish, N. J. & Poujade, O. Forward modeling of space-borne gravitational wave detectors. *Physical Review D* **69**, 082003 (2004). URL <https://link.aps.org/doi/10.1103/PhysRevD.69.082003>. 0311069.
20. Cutler, C. Angular resolution of the LISA gravitational wave detector. *Physical Review D* **57**, 7089–7102 (1998). URL <https://link.aps.org/doi/10.1103/PhysRevD.57.7089>. gr-qc/9703068.
21. Roebber, E. *et al.* Milky Way Satellites Shining Bright in Gravitational Waves. *The Astrophysical Journal* **894**, L15 (2020). URL <https://iopscience.iop.org/article/10.3847/2041-8213/ab8ac9>. 2002.10465.

22. Karnesis, N., Babak, S., Pieroni, M., Cornish, N. & Littenberg, T. Characterization of the stochastic signal originating from compact binary populations as measured by LISA. *Physical Review D* **104**, 043019 (2021). URL <https://link.aps.org/doi/10.1103/PhysRevD.104.043019>.